NASA TM X-378

TECHNICAL MEMORANDUM

X-378

CONVECTIVE HEAT TRANSFER TO A BLUNT LIFTING BODY

By John O. Reller, Jr., and H. Lee Seegmiller

Ames Research Center
Moffett Field, Calif.

NATIONAL AERONAUTICS AND SPACE ADMINISTRATION
WASHINGTON
September 1960

NATIONAL AERONAUTICS AND SPACE ADMINISTRATION

TECHNICAL MEMORANDUM X-378

CONVECTIVE HEAT TRANSFER TO A BLUNT LIFTING BODY*

By John O. Reller, Jr., and H. Lee Seegmiller

SUMMARY

An investigation has been made of the convective heat-transfer characteristics of a blunt lifting shape and of some of the effects of enthalpy level on local heating rates. Measurements in conventional and shock-driven wind tunnels at Mach numbers from 5 to 9 and stagnation enthalpies up to 5,300 Btu/lb are compared with theoretical predictions at Mach numbers and enthalpies characteristic of the high-heating portion of a typical entry trajectory. The distribution of heating rates around a blunt lifting shape is shown to be relatively unaffected by enthalpy level and to compare favorably with theory for equilibrium real-gas flow. It is also shown that control surfaces extending out from the body surface can experience heating rates which exceed those occurring in the body stagnation region. In general, it appears feasible to predict equilibrium convective heat transfer to most body and control surfaces of full-scale blunt lifting shapes during the high-heating portion of an entry trajectory by use of existing theory, along with experimental surveys at relatively low enthalpy levels.

INTRODUCTION

A class of relatively blunt shapes which develop sufficient aerodynamic lift during atmosphere entry to gain some flexibility of operation has been discussed in reference 1. However, these shapes give rise to more complex aerodynamic-heating problems than do simple ballistic vehicles since the shapes themselves are more complicated and since either angle of attack or control-deflection angle may be varied in flight to achieve the desired trajectory. Such changes in flight attitude may cause substantial variations in heating on both body and control surfaces. The purpose of the present investigation is to examine this situation as it relates to a blunt, 30° half-cone shape, introduced in reference 2, and to inquire into methods by which its heating characteristics can be predicted or measured.

*Title, Unclassified

SYMBOLS

A	reference area
C_D	drag coefficient
C_p	pressure coefficient
c_p	specific heat at constant pressure
D	drag force
d	maximum body diameter
H	enthalpy
h	heat-transfer coefficient, $\frac{\dot{q}c_{p_2}}{(H_{aw} - H_w)A}$ or $\frac{\dot{q}}{(T_{aw} - T_w)A}$
k	thermal conductivity of gas
L	lift force
l	axial distance from nose of body
M	Mach number
N_{St}	Stanton number, $h/\rho U c_p$
N_{Pr}	Prandtl number, $c_p\mu/k$
$\dot{q}$	heat-transfer rate
R	Reynolds number, $\frac{\rho U(\text{Length})}{\mu}$
S	surface distance from geometric stagnation point, or circumferential surface distance from lower meridian
T	temperature
t	time

U	velocity
W	glide weight
Y	distance normal to body surface
α	angle of flat top surface relative to free-stream direction
δ	control-deflection angle
ρ	density of gas
μ	absolute viscosity

Subscripts:

aw	adiabatic wall
d	referenced to maximum body diameter
r	based on nose radius of curvature
s	stagnation
w	wall, body surface
2	referenced to conditions behind normal shock
TE	trailing edge

RESULTS AND DISCUSSION

Typical Entry Trajectory

The convective-heating-rate history of the blunt, 30° half-cone shape of the present investigation in a typical entry trajectory from a circular orbit is shown in figure 1. The body has a maximum diameter of 10 feet, a value of W/C_DA of 95 lb/sq ft, and develops a lift-drag ratio of 0.33. Stagnation heating rate $\dot{q}_s$ and enthalpy H_s are shown as a function of time from the initiation of entry to indicate the range of heating conditions encountered. Maximum heating rates are about 70 Btu/(sq ft)(sec), with stagnation enthalpies up to 12,000 Btu/lb. The heating curve has a flat, dished region due to a slow oscillation or "skip" imposed by the requirement (in this trajectory) of a constant L/D glide following the prescribed reverse-thrust phase. At several

locations on the heating-rate curve are shown the flight Mach numbers, while the corresponding Reynolds numbers based on body diameter are presented in a table on the figure. Maximum heating is seen to occur between $M = 26$ and $M = 14$, as R_d increases from 70,000 to just over 1/2 million. In this relatively low Reynolds number range, it is expected that boundary-layer flow would be essentially laminar.

One additional point must be mentioned with regard to the convective heat-transfer environment. This point has to do with the equilibrium state of the gas. The results of an investigation conducted at Ames Research Center by Paul M. Chung show that, for the range of flight conditions indicated in figure 1, both the inviscid flow and the viscous boundary-layer flow enveloping much of the body can depart substantially from the equilibrium real-gas state because of the time lag in chemical recombination. The resultant effect on local heating rates will not be large, however, if the surface is highly catalytic in the sense that it promotes recombination. In fact, for the case of a relatively cold metallic surface (less than $2,000^\circ$ R) the heating rates should approach those for equilibrium flow as an upper boundary. If the surface is noncatalytic, for example, a plastic or a glass, a considerable reduction in local heating rates can occur because of the lag in recombination at the surface.

From these considerations then, the heating characteristics of this configuration can be studied in conventional wind tunnels, provided the direct effects of enthalpy level can be determined. To determine some of these effects, tests were conducted with the model shown in figure 2. The configuration is essentially one-half of a blunt cone with a semiapex angle of 30°. Flap-type controls extend from the base and are offset from the body center line. Elevon controls were also tested and are shown in a subsequent figure. Reference 1 has presented a few of the aerodynamic force and moment characteristics of this configuration; additional information will be found in reference 3. Tests were conducted in the Ames 10- by 14-inch supersonic wind tunnel at $M = 5$ and at the low value for H_s of 160 Btu/lb and in the Ames 1- by 1-foot hypervelocity shock tunnel at $M \approx 9$ and $H_s \approx 4,000$ Btu/lb. (Note that this latter enthalpy corresponds to a Mach number of about 12 in the flight trajectory of fig. 1.) In both test facilities, thin shell models were used to obtain heating rates by the transient temperature technique. Thermocouple signals were first amplified and then recorded by an oscillograph.

Figure 3 presents two self-illuminated time exposures of one of these models in the shock tunnel. In the vicinity of the body and over both controls can be seen the bright glow of the shock-heated incandescent gas. The outline of the body shock wave can be seen, while in figure 3(b) the rear of the model is illuminated by reflected light from the support system. The camera shutter was closed at about 100 milliseconds after

the start of flow, at which time the model was still enveloped in the high-enthalpy airstream. Although the stagnation enthalpy for this test condition is only about one-third the maximum value desired for the present study, it is sufficiently high to indicate some of the trends in heat transfer with enthalpy. Reynolds numbers were sufficiently low in both facilities so that boundary-layer flow was apparently laminar in all cases.

Stagnation Heat Transfer

Some of the results obtained in these tests as they relate to stagnation-point heat transfer are shown in figure 4 in which the dimensionless heating parameter $(N_{St})_2(N_{Pr})_2^{2/3}(R_r)_2^{1/2}$ is shown as a function of stagnation enthalpy. The parameter is referenced to conditions behind the normal shock wave with high-temperature gas properties evaluated from reference 4. The circular test-point symbols on figure 4 are data for the present configuration, and the square test-point symbols represent tests of the Project Mercury capsule configuration at the Ames Research Center both in the 10- by 14-inch supersonic wind tunnel and the 2-inch hypervelocity shock tunnel at stagnation enthalpies between about 5,000 and 5,300 Btu/lb. The data are compared with the theory of Fay and Riddell (ref. 5) which was applied to a wide range of conditions (M from 4 to 26 and H_s from 160 to almost 12,000 Btu/lb) that pertain to the three test facilities and the flight trajectory shown previously. Also shown in figure 4 are the two Mach numbers, 14 and 26, which bracket the high heating portion of the trajectory shown in figure 1; the test data extend into the lower part of this region. The theoretical variation, which shows only a moderate dependence on enthalpy, is represented by the shaded region. This shaded area indicates a spread of ±5 percent in the theoretical estimates which may, in part, be due to our imperfect knowledge of the real-gas properties. Theory and experiment are in good agreement both at the low enthalpies and at moderate enthalpies from 4,000 to 5,000 Btu/lb. Indeed, the experimental results seem to support the indicated theoretical trend. These results suggest, then, that the estimation of heating rates to the stagnation region of a full-scale vehicle of the blunt ballistic or lifting type during the high heating portion of an entry trajectory should be possible with reasonable accuracy.

L 1094

Heating-Rate Distribution

Top and bottom body meridian at $\alpha = 0^\circ$.- The distribution of heating rate over the surface of the body was also investigated. Local heating rates at $\alpha = 0^\circ$, referenced to the stagnation value, are presented in figure 5 as a function of normalized surface distance along the top and bottom meridian of the body. Heat-transfer data obtained

in the low-enthalpy airstream (circular test-point symbols) are compared with the theories of Lees (ref. 6) and Van Driest (ref. 7) for a laminar boundary layer. The theoretical results were obtained by using the measured surface pressures of reference 3 and are in general agreement with the measured heating rates. One exception, however, is the point on the small upper radius of the nose, where the measured rate exceeded the stagnation-point value. Now, it should be noted that the low-enthalpy test results were obtained in the form of heat-transfer coefficients. However, by referencing the local coefficient to the stagnation value as the ratio h/h_s and by using the "cold wall" assumption, these data for this blunt shape can be interpreted as the ratio of heating rates $\dot{q}/\dot{q}_s$. As such, they are comparable, within the experimental accuracy, with the heating-rate ratios obtained in the high-enthalpy tests and from theory.

The square test-point symbols in the figure represent results obtained in the Ames 1- by 1-foot hypervelocity shock tunnel in a stream whose enthalpy was about 4,000 Btu/lb. As can be seen in the figure the agreement between the two sets of data is quite favorable in the stagnation region and on the lower surface. On the upper surface, the high-enthalpy data are substantially lower, a fact which is attributed to the relatively lower pressure level in this region caused by the difference in Mach number as well as in enthalpy level.

Finally, in this figure the dashed lines represent the heating distribution at the conditions of $M = 22$ in the reference trajectory. It will be recalled that $M = 22$ is in the region of maximum convective heating for this trajectory. These results were obtained from the theory of Kemp, Rose, and Detra (ref. 8) with the use of Newtonian pressures, and that of Romig and Dore (ref. 9) for both Newtonian and blast-wave pressures (ref. 10). Substantial agreement with the previous results is apparent although these equilibrium real-gas predictions are somewhat lower on the conical section. On the top surface, the predictions for $M = 22$ bracket the shock tunnel data, and it is difficult to say which is more realistic.

Circumferential direction at $\alpha = 0^\circ$.- The variation of local heating rates in a circumferential direction at several locations on the body is shown in figure 6 for $\alpha = 0^\circ$. The symbol S represents surface distance from the lower body meridian, while S_T is one-half the local circumference. The symbols l and l_T refer to axial distances. The conical region, the top leading edge, and the flat top surface of the body are identified in the figure. Data are shown for both enthalpy levels, $H_s = 160$ and 4,000 Btu/lb, while ideal-gas theory for a laminar boundary layer is presented for the rearward position, $l/l_T = 0.75$. The low-enthalpy data at this location are seen to compare favorably with the theoretical prediction, which is based on measured

pressures. Also at $l/l_T = 0.45$ the high- and low-enthalpy data are in agreement in the conical region. On the leading edge and top surface, the high-enthalpy data fall considerably below the heating-rate level for the low-enthalpy data, a fact which has been noted previously in figure 5. Notice also that the top leading edge of the body does not experience high heating rates, at least at this angle of attack, despite its relatively small radius of curvature. In fact, the heating distribution in this region is similar to that for a yawed cylinder.

Variation with angle of attack.- The variation of local heating rates at several points on the body with angle of attack is presented in figure 7. Angle of attack α is measured relative to the top surface. Figure 7(a) shows the locations and test-point symbols for the data in figure 7(b). The angle-of-attack range from -17° to 7° represents trimmed flight at L/D ratios from 0.2 to 0.5. The top curve shows data for the tangent point of the small upper nose radius, where rates up to 20 percent above the normal stagnation value were measured. The square and triangular test-point symbols represent locations about halfway around the top leading edge; the first, on the meridian line where the leading-edge sweep is 0°, and the second, farther back where the leading-edge sweep is 60°. Despite the small radius of curvature, this region is not a critical heating area. Other curves show the expected trends for the lower conical and upper flat surfaces. The solid diamond test-point symbols at $\alpha = 0^\circ$ and $\alpha = 4^\circ$, which are shock-tunnel data points for the conical surface, should be compared with the dashed curve, which is the low-enthalpy heating level for the same location on the body. High-enthalpy data for the leading edge and top surface are lower than comparable low-enthalpy values because of the combined Mach number and enthalpy effect noted previously. In general, these results show that angle of attack does not have a pronounced effect on heating rates for the blunt body tested.

Summary statement.- On the basis of the results discussed so far, in particular, the stagnation-point correlation, the similarity in heating-rate distribution at several enthalpy levels, and the general agreement between theory and experiment in regions where reliable comparisons can be made, it appears that low-enthalpy heating-rate measurements can be used as a basis from which to predict, with reasonable accuracy, the full-scale equilibrium convective-heat-transfer rates over most of the surfaces of a blunt lifting shape. (It must be recalled, however, that in flight a noncatalytic wall condition may reduce the actual heating rates below these predicted values.) Probable exceptions to this general statement are regions of separated flow, such as at the base of this configuration. Heating rates in this region have, to date, only been measured at the low-enthalpy level. Recorded values were from 1 to 5 percent of the stagnation heating rate. These preliminary results are not conclusive, however, since extrapolation to the enthalpy level

of the full-scale vehicle involves nonequilibrium real-gas effects that are difficult to predict.

Control-Surface Heating

Body pressure field.- Before the heat-transfer characteristics of the flap-type controls are examined, the flow field surrounding the body in which the controls operate will be considered. Some results from a pitot-pressure survey rake located at the base of the body and representative measured control pressures are presented in figure 8. The abcissa in both parts of the figure is a nondimensional distance normal to the body surface. Consider first the pitot-survey-rake data shown in the left part of the figure. At the bottom and side of the body, the low-energy air originating at the normal or nearly normal portion of the body shock wave was apparently confined for the most part to a thin layer at the body surface. In this area, at $Y/d < 0.04$, the pressure coefficient must rise from a value near 1.8 at the edge of the boundary layer to the measured value of 4.8 at the location of the first orifice. This latter value approaches the theoretical limit of about 5.2 for isentropic compression behind the oblique shock wave generated by the conical surface. The measured values decrease as the shock wave is approached since the local Mach number is increasing. The lower limit (dashed line) corresponds to the pitot-pressure coefficient for the Mach number just behind the oblique shock wave. The two outermost orifices were outside of the body shock wave and recorded normal shock pressures.

For the upper pitot survey rake, all four orifices were within the body shock wave and recorded a gradually rising pressure with increasing value of Y. The curve through the data fairs into the theoretical value (from Prandtl-Meyer expansion of flow behind normal shock) at the body surface, $Y = 0$. Such pressure variation would be expected downstream of a continuously curving shock wave.

On the right side of figure 8, the range of pressures measured on the flap-type controls is presented in coefficient form. The parameter Y_{TE}/d is the nondimensional distance, normal to the body surface, to the flap trailing edge. The upper and lower solid curves in each set are, respectively, the maximum and minimum pressure curves. The vertical bars and test-point symbols correspond to measured data at control-deflection angles of 0°, 30°, 60°, and 90° on the upper control and 0°, 30°, and 60° on the lower, where δ is measured from a normal to the base of the model. The dashed portion of the curves for the lower control is an extrapolation to $\delta = 90^\circ$ based on the two theoretical limits shown in the left part of the figure. In general, the lower control experienced higher pressures. Note that at high deflection angles both the upper and lower controls were subject to pressures in excess of the

normal stagnation value and that large gradients occurred. These results are related to the extension of the controls into the high-energy flow discussed previously, which passes through the oblique portions of the body shock wave. This of course implies that the low-energy layer which originates in the normal shock region at the nose does not protect the controls in the same fashion that it does the body surface. This effect is attributed, in part, to a two-dimensional flow over the controls from the center toward the edges which bleeds off the low-energy layer.

It is somewhat surprising that the upper controls experienced these large pressures since they are not indicated by the pitot survey rake. Note, however, that the controls are offset from the body center line, which is the location of the pitot survey rake. Inspection of the pressure distribution on the controls indicated that a large pressure gradient must exist parallel to the base, which, in combination with the control offset, would explain this difference. In view of these findings, then, it might be expected that both upper and lower control-surface heating rates would also vary widely.

Heat transfer to flap-type controls.- Heat-transfer rates to the flap-type controls, referenced to the body stagnation value, are presented as a function of control-deflection angle δ in figures 9 and 10. The angle δ is defined by the small sketches. In figure 9, experimental data and theory are for the outboard trailing edge of the controls, at the locations indicated by the dots in the sketch at the upper right. Three-dimensional laminar boundary-layer theory based on wedge and Newtonian impact pressures is used for comparison (solid curves), with local Reynolds numbers referenced to the length from the flap leading edge. The dashed curves are similar heating estimates based on measured control pressures. The experimental low-enthalpy heating rates to the trailing edge of both the upper and lower control (circular test-point symbols) are seen to depart substantially from those predicted using Newtonian theory at values of δ greater than 20° and to follow the estimated trend based on measured pressures. On the lower control, the indicated heating rate exceeded that of the body stagnation point at a value of δ of about 50°. On the upper control, the relatively high measured values at low values of δ are attributed to body cross-flow effects. Two data points from the shock tunnel at $\delta = 45^\circ$ are shown (square test-point symbols). The measured value on the lower control agrees with the low-enthalpy result. On the upper control, however, a considerably higher heating rate was measured, which may be indicative of a change in the body cross-flow pattern at the high-enthalpy test conditions.

In figure 10, the shaded areas represent the range of heating rates encountered on the control surfaces at each deflection angle. The data points are the same as those shown in figure 9. Substantial heating gradients are apparent. The shaded areas indicate that the highest heating rate was usually forward of the trailing edge, although the

location of the point of maximum heating has been found to vary with control-deflection angle. Note that the high-enthalpy data for the upper control at $\delta = 45^\circ$ extend into the low-enthalpy range of measured heating rates. The maximum measured rate for these tests was on the lower control at $\delta = 60^\circ$ and was 80 percent greater than the body stagnation value.

Heating rates to the lower controls are presented as a function of angle of attack in figure 11. Data are shown for deflection angles of 0°, 20°, 30°, 45°, and 60°. The angle-of-attack range is from -14° to 7°. It is seen that the general level of heating remains unchanged with angle of attack, although the pattern is somewhat erratic. A similar erratic behavior has been noticed in the measured heating rates to the upper controls. Additional shock-tunnel tests are now in progress and will provide high-enthalpy data at several control-deflection angles and several body angles of attack. Also, a theoretical study of both control pressures and heating rates is underway to evaluate methods of predicting control heating rates at the flight-enthalpy level.

On the basis of present results, it would seem possible to extrapolate control-heating data to the enthalpy level of the full-scale vehicle, much in the same manner as for the body surfaces.

Heat transfer to elevon controls.- Some representative low-enthalpy elevon-heating data are shown in figure 12, where the ratio $\dot{q}/\dot{q}_s$ is given as a function of angle of attack for an elevon deflection angle of 0°. A two-view sketch of these controls giving linear dimensions is shown at the right. It will be noted that the leading-edge radius is 0.02d, which is only 10 percent of the body nose radius. The data presented are the average of three values measured at different locations on the leading edge or flat surfaces. On the leading edge of the control there was considerable variation in the measured rates, and in several instances at negative α one of the values was in excess of the body stagnation heating rate; thus the presence of the high-energy airflow discussed previously was indicated. As with the flap-type controls, the variation of elevon heating rate with angle of attack is erratic. The lower two curves for the upper and lower control surfaces intersect near $\alpha = 0^\circ$ and appear to vary in a predictable fashion with angle of attack at values from 0.1 to about 0.3 of the reference heating rate. Additional elevon heating data have been obtained at deflection angles from -30° to 30°. Preliminary inspection of these data has revealed upper- and lower-surface heating rates ranging up to about 3/4 of the reference value. Leading-edge values, on the other hand, were relatively unaffected by variation in deflection angle.

These preliminary elevon-heating results indicate that a control of this type will encounter sizable heating rates on leading-edge and

windward surfaces. Local values can approach or exceed that measured at the stagnation point of the body and would appear to result, as was the case for the flap-type controls, from immersion of the control in the high-energy portion of the body flow field rather than in the flow originating at the normal shock wave at the nose.

CONCLUDING REMARKS

This paper has reported an investigation of the convective heat-transfer characteristics of a blunt lifting shape and has examined some of the effects of enthalpy level on these heating characteristics. Heating rates were measured in conventional and shock-driven wind tunnels at stagnation enthalpies up to 5,300 Btu/lb. Stagnation-heating rates have been correlated with theory in a manner that shows only a moderate dependence on enthalpy level. The distribution of heating rates around a blunt lifting shape has been shown to be relatively unaffected by enthalpy level and to compare favorably with theory for equilibrium real-gas flow. It has further been shown that control surfaces extending into the flow field around a blunt lifting shape will encounter relatively high-energy airflow and can experience heating rates which exceed that occurring at the stagnation point of the body. In summary of these results, it appears feasible to use existing theory, along with experimental surveys at relatively low enthalpy levels, to predict equilibrium convective heat transfer to most body and control surfaces of full-scale blunt lifting shapes during the high-heating portion of an entry trajectory.

Ames Research Center
National Aeronautics and Space Administration
Moffett Field, Calif., April 11, 1960

REFERENCES

1. Dennis, David H., and Edwards, George G.: The Aerodynamic Characteristics of Some Lifting Bodies. NASA TM X-376, 1960

2. Eggers, Alfred J., Jr., and Wong, Thomas J.: Re-Entry and Recovery of Near-Earth Satellites, With Particular Attention to a Manned Vehicle. NASA MEMO 10-2-58A, 1958.

3. Sarabia, Michael F.: Aerodynamic Characteristics of a Blunt Half-Cone Entry Configuration at Mach Numbers From 3 to 6. NASA TM X-393, 1960

4. Hansen, C. Frederick: Approximations for the Thermodynamic and Transport Properties of High-Temperature Air. NACA TN 4150, 1958.

5. Fay, J. A., and Riddell, F. R.: Theory of Stagnation Point Heat Transfer in Dissociated Air. Jour. Aero. Sci., vol. 25, no. 2, Feb. 1958, pp. 73-85, 121.

6. Lees, Lester: Laminar Heat Transfer Over Blunt-Nosed Bodies at Hypersonic Flight Speeds. Jet Propulsion, vol. 26, no. 4, Apr. 1956, pp. 259-269.

7. Van Driest, E. R.: The Laminar Boundary Layer With Variable Fluid Properties. Rep. No. AL-1866, North Americal Aviation, Inc., Jan. 19, 1954.

8. Kemp, Nelson H., Rose, Peter H., and Detra, Ralph W.: Laminar Heat Transfer Around Blunt Bodies in Dissociated Air. Res. Rep. 15, AVCO Res. Lab., May 1958.

9. Romig, Mary F., and Dore, F. J.: Solutions of the Compressible Laminar Boundary Layer Including the Case of a Dissociated Free Stream. Rep. ZA-7-012, CONVAIR, Aug. 4, 1954.

10. Lees, Lester, and Kubota, Toshi: Inviscid Hypersonic Flow Over Blunt-Nosed Slender Bodies. Jour. Aero. Sci., vol. 24, no. 3, Mar. 1957, pp. 195-202.

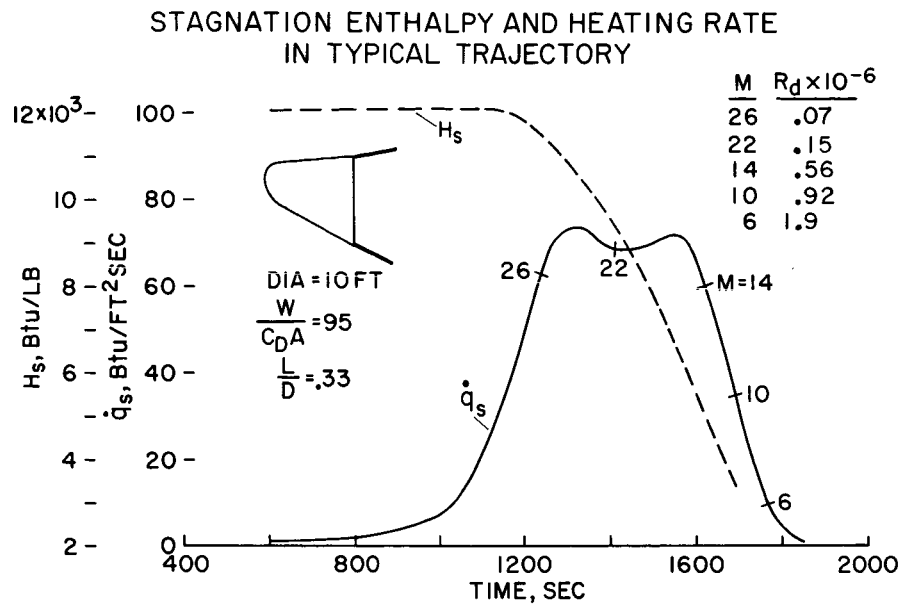

Figure 1

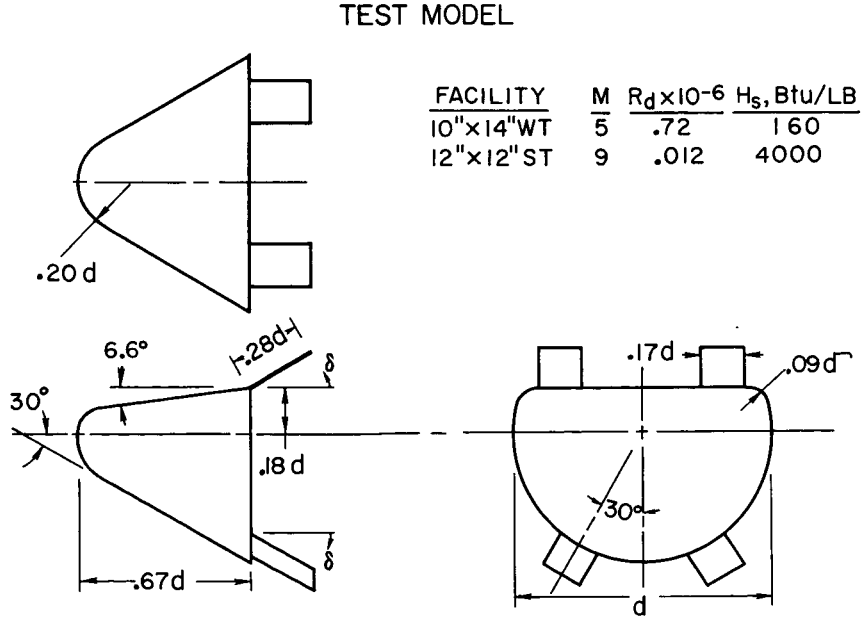

Figure 2

TEST MODEL IN HIGH ENTHALPY AIR STREAM
SIDE VIEW

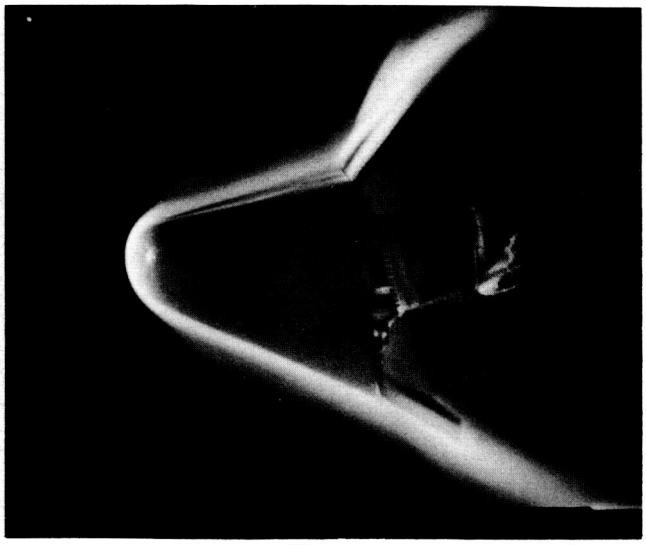

Figure 3(a)

TEST MODEL IN HIGH ENTHALPY AIR STREAM
REAR VIEW

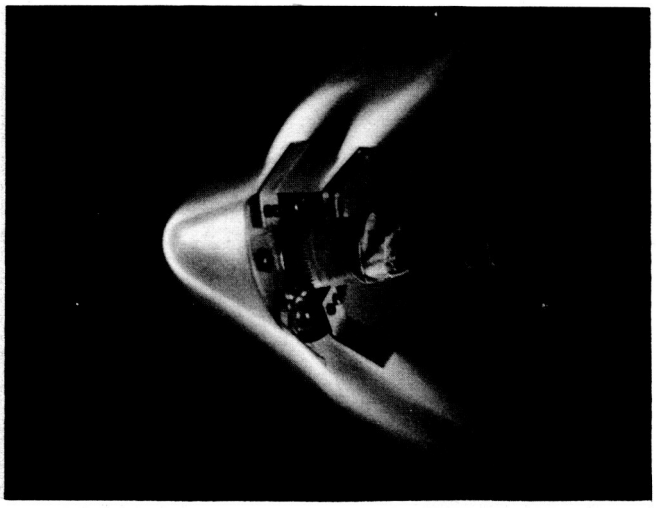

Figure 3(b)

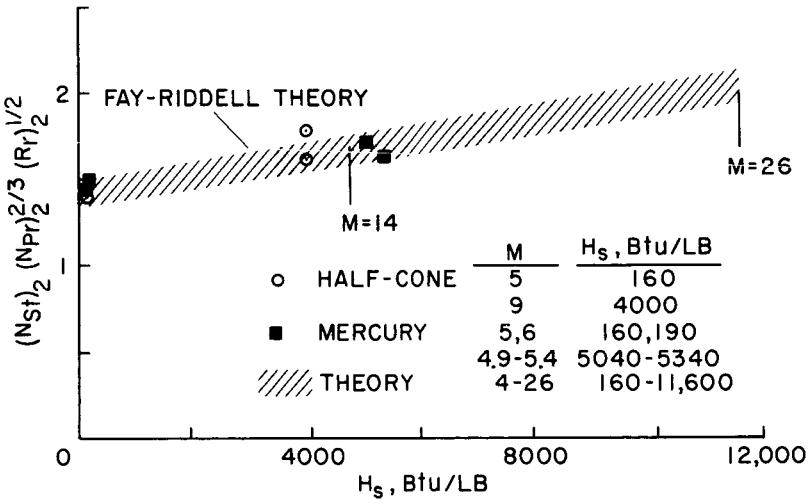

Figure 4

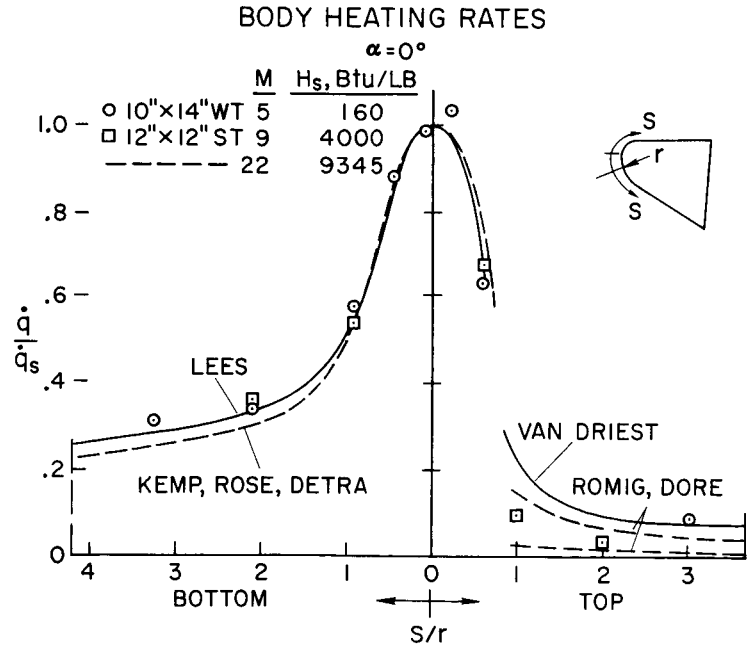

Figure 5

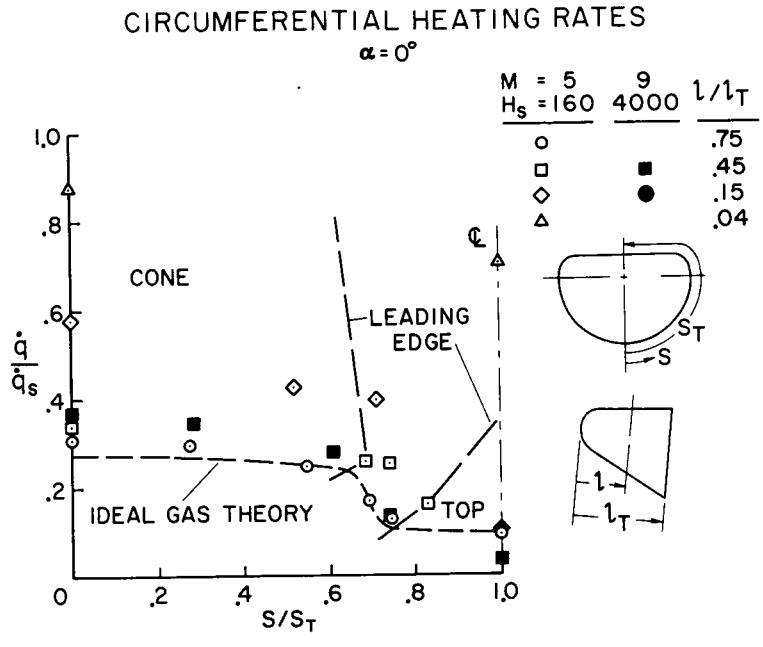

Figure 6

LOCATIONS FOR HEAT-TRANSFER MEASUREMENTS

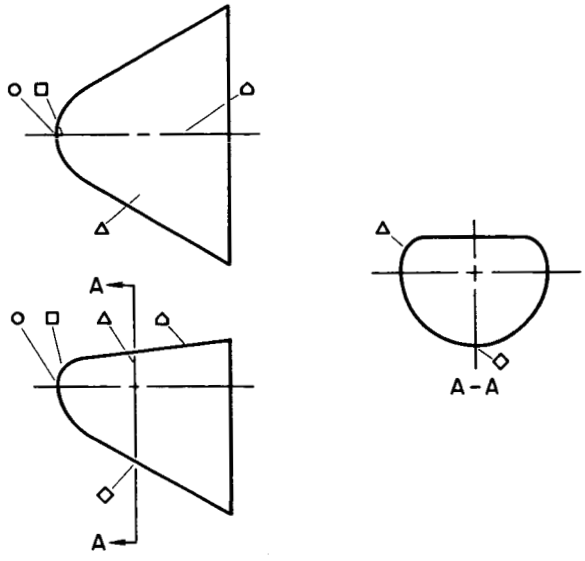

Figure 7(a)

BODY HEATING RATES

α = -17° TO 7°

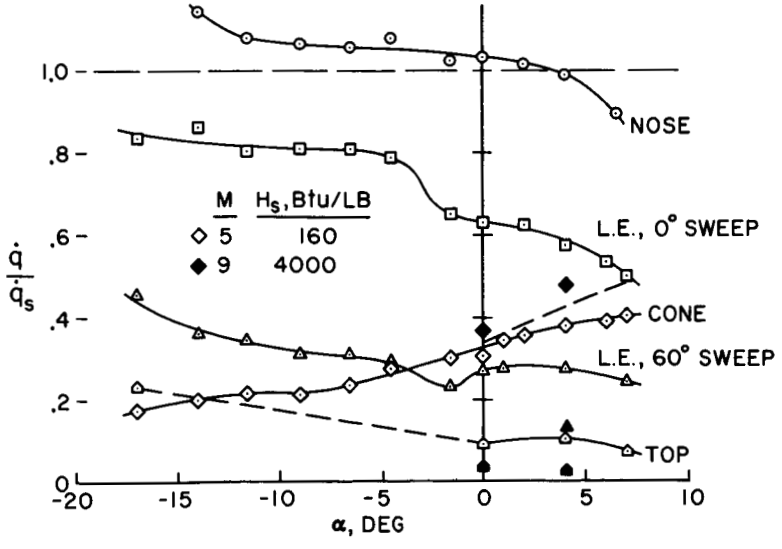

Figure 7(b)

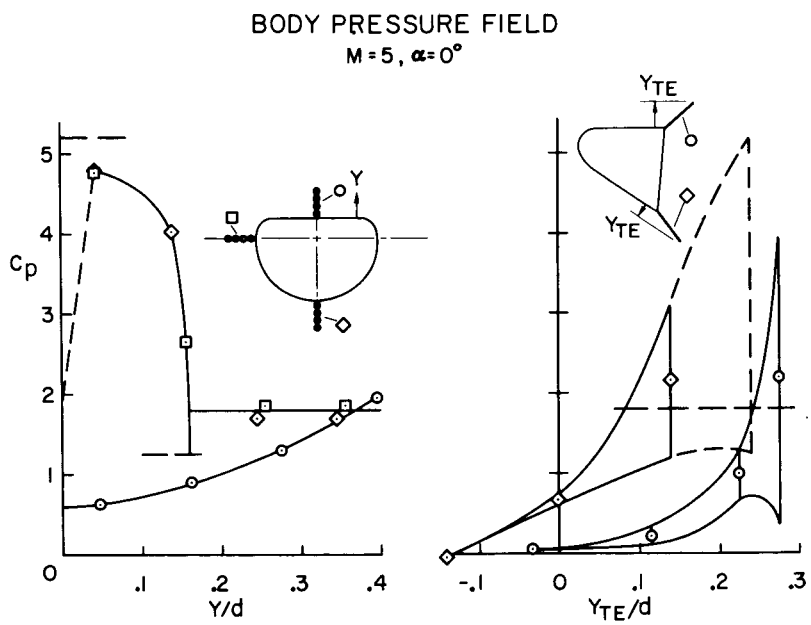

Figure 8

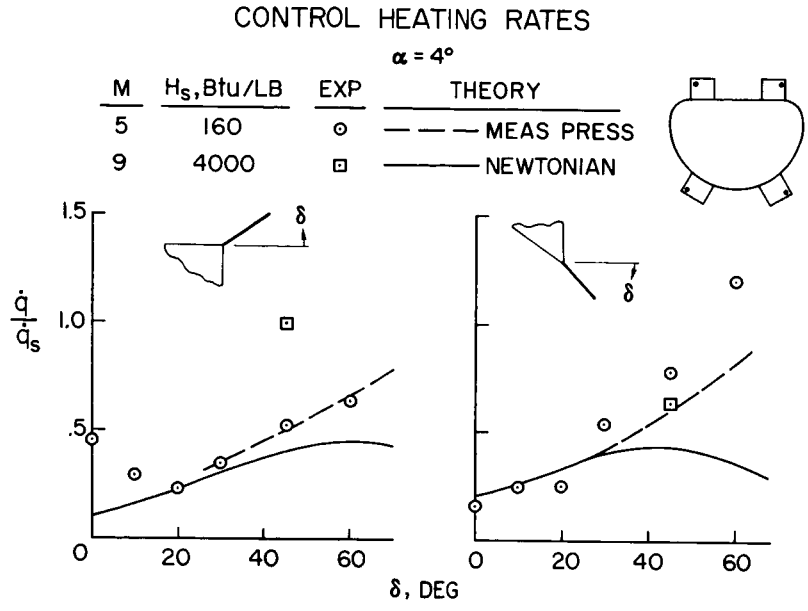

Figure 9

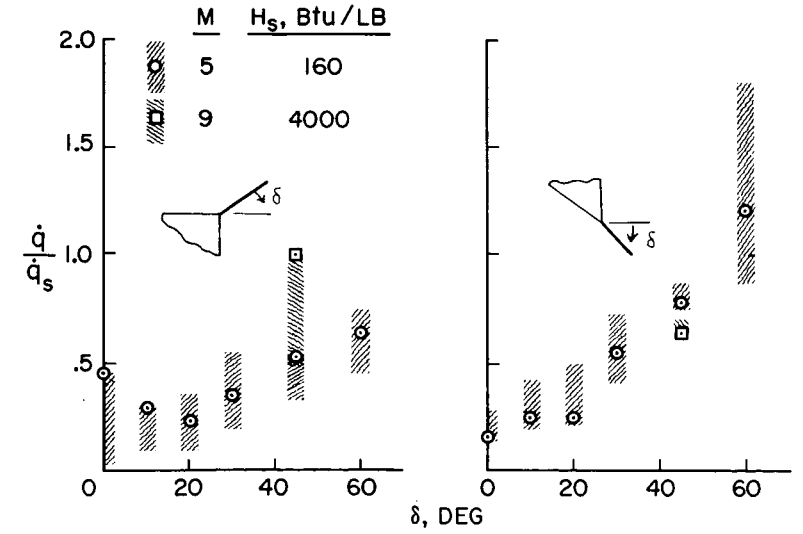

Figure 10

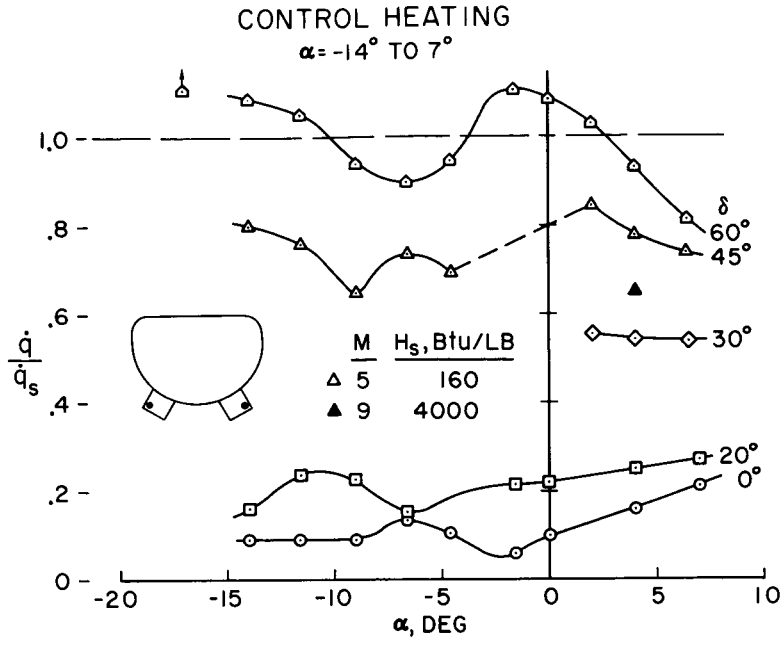

Figure 11

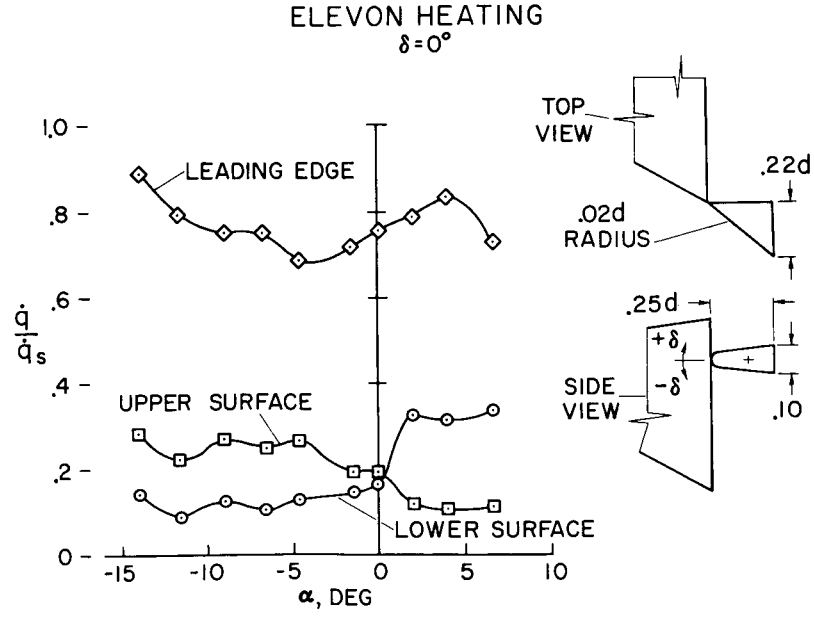

Figure 12